Polish J. Chem., **78**, 1221–1234 (2004)

On the Role of Specific Characteristics of the Streaming Mercury Electrode in the Generation of the Nonlinear Electrochemical Dynamical Phenomena*

by M. Orlik and R. Jurczakowski**

Laboratory of Electroanalytical Chemistry, Department of Chemistry, University of Warsaw, ul. Pasteura 1, PL-02-093 Warsaw, Poland

(Received February 28th, 2004)

The streaming mercury electrode was recently found by us a very powerful electrode type for the observation of sustained oscillations and multistability accompanying the electrode processes with the region of the negative differential resistance (NDR) in their *I-E* characteristics. Following our earlier experimental and theoretical studies of the electroreduction of the pseudohalogenide complexes of nickel(II) at the streaming mercury electrode, we discuss the conditions for the onset of oscillations and multistability in these processes, taking into account the dependence of the double layer capacitance on the electrode potential. The improved stability criteria, involving both the differential C_d and integral K capacitances are derived and compared with our earlier simplified theory. Based on the experimental characteristics of the Ni(II)-SCN^- electroreduction it is quantitatively shown, how the two factors specific to the streaming electrodes: the permanent flow of the capacitive current and – in particular – the relatively small thickness of the diffusion layer determine the characteristics of the bistable and oscillatory behaviour.

Key words: streaming mercury electrode, double layer capacitance, equivalent circuit, nonlinear dynamics, electrochemical oscillations, bistability

In our recent papers [1–3] we described the application of the streaming mercury electrode as a very powerful electrode type for the studies of sustained oscillations and multistability in the electroreduction of the thiocyanate [1] and azide [3] complexes of nickel(II) which processes exhibit the region(s) of the negative differential resistance (NDR) in their *I-E* characteristics. Such an electrode type, although known for many years [4], was never applied before for the studies of oscillations or multistability in any electrode process. Therefore in our papers we not only reported the representative experimental results, but also elaborated the generalized theoretical stability analysis [2,3] of the processes of the type studied. Although our derivations were based on certain simplifications, including, among others, the potential-independent double layer capacitance, the theoretical bifurcation diagrams agreed quite well with the experimental ones [2,3].

---

* Dedicated to Prof. Dr. Z. Galus on the occasion of his 70th birthday.

** Author to whom all correspondence should be addressed. E-mail: morlik@chem.uw.edu.pl

For the Ni(II)-SCN^- electroreduction the stability diagram consisted of a tiny loop of the oscillatory region expanding into a relatively large region of bistability (*cf*. Figure 6 in [2]). In the creation of such a shape, besides the characteristics of the electrode process, the role of two principal factors, specific only to the streaming electrodes, can be considered:

(i) the permanent flow of the capacitive current which is a source of a *qualitatively new* mathematical term in the stability criteria for the streaming electrodes, and

(ii) the relatively small (*ca*. 1–2 μm for the conditions of our experiments) thickness of the diffusion layer, associated with the appropriately fast reactant transport; this factor has a *quantitative* nature, as the diffusion layer exists for all the electrode types.

In view of the above, the aim of this paper is to analyse the role of these specific characteristics of the streaming electrodes in determination of the shape of the bifurcation diagram for such electrodes, taking the Ni(II)-SCN^- electroreduction [1,2] as an experimental example. Also, in conjunction with the role of the capacitive current we derive and discuss the improved general stability criteria of processes at the streaming electrode.

EXPERIMENTAL

The equipment and reagents used for collecting the experimental data at the streaming mercury electrode were described in Refs. [1,5,6]. In particular, the double layer capacitances of Hg in contact with 2 mol dm^{-3} NaSCN were determined with the use of the ac OH-105 polarograph (Radelkis, Hungary). The dropping mercury electrode was used as a working electrode, the potential of which was controlled vs. the calomel electrode $Hg|Hg_2Cl_2|KCl$(sat.), separated from the studied solution by a salt bridge. The Pt plate of a surface area 2 cm^2 served as an auxiliary electrode. The ac currents recorded at frequency $f = 60$ Hz for the ac amplitude 2 mV were recalculated into the corresponding capacitances by comparison with ac currents for the 0.1 mol dm^{-3} KCl solution of published $C_d(E)$ data [7].

Numerical calculations were done in Pascal with the IBM PC compatible Pentium IV machine.

THEORY

The capacitive current in terms of the integral and differential double layer capacitance. For the analysis of the role of the capacitive current in the system's stability it is first useful to describe this current more strictly than it was done before [2,3]. In those papers, for simplification of the mathematical derivations, we invoked not the potential-dependent, but either *constant differential* C_d [2] or *constant integral* K [3] double layer capacitance.

Let Q_{dl} denote the double layer charge that is necessary for the electrode of a surface area A to acquire the externally imposed potential E (if different from the potential of zero charge E_{pzc}). The integral double layer capacitance *per unit area* (denoted in literature with K or C_i [8]), is related to the differential capacitance per unit area $C_d = A^{-1}(dQ_{dl}/dE)_E$ according to the following expression [8]:

$$K(E) = \frac{1}{E - E_{\mathrm{pzc}}} \int_{E_{\mathrm{pzc}}}^{E} C_{\mathrm{d}}(E)\mathrm{d}E \tag{1}$$

In view of that relationship it is clear that if in our earlier works we assumed, for simplification, the constant (average) differential capacitance C_{d}, this automatically implied the same value for the integral capacitance K, similarly as the assumption on the constant integral capacitance implied the same value of the differential capacitance.

According to the definition of the integral double layer capacitance (1), when the (ideal) streaming electrode of a given surface area is charged from the point of zero charge E_{pzc} to the given potential E, the corresponding charge Q_{dl} is given by Equation (2):

$$Q_{\mathrm{dl}} = 2\pi r l_{\max} K(E) \times (E - E_{\mathrm{pzc}}) \tag{2}$$

where $A = 2\pi r l_{\max}$ is a side surface area of the cylindrical mercury stream of a radius r and total length $l_{\max}$. The capacitive current $I_{\mathrm{c}} = \mathrm{d}Q_{\mathrm{dl}}/\mathrm{d}t$ may then be calculated [9] and expressed in the form of Equation (3), with $v = \mathrm{d}l/\mathrm{d}t$ being the flow velocity of mercury stream:

$$I_{\mathrm{c}} = \frac{\mathrm{d}Q_{\mathrm{dl}}}{\mathrm{d}t} = 2\pi r v K(E) \times (E - E_{\mathrm{pzc}}) + 2\pi r l_{\max} (E - E_{\mathrm{pzc}}) \frac{\mathrm{d}K}{\mathrm{d}E} \frac{\mathrm{d}E}{\mathrm{d}t} + 2\pi r l_{\max} K \frac{\mathrm{d}E}{\mathrm{d}t} \tag{3}$$

For the purposes of our analysis it is also useful to calculate the derivative $\mathrm{d}K/\mathrm{d}E$:

$$\frac{\mathrm{d}K}{\mathrm{d}E} = \frac{\mathrm{d}}{\mathrm{d}E}\left[\frac{1}{E - E_{\mathrm{pzc}}} \int_{E_{\mathrm{pzc}}}^{E} C_{\mathrm{d}}(E)\mathrm{d}E\right] = \frac{C_{\mathrm{d}}(E) - K(E)}{E - E_{\mathrm{pzc}}} \tag{4}$$

The combination of Equation (3) with Equation (4) yields the following final expression for the total capacitive current at the streaming electrode, valid for dc conditions:

$$I_{\mathrm{c}} = 2\pi r v K(E) \times (E - E_{\mathrm{pzc}}) + 2\pi r l_{\max} C_{\mathrm{d}}(E) \times \frac{\mathrm{d}E}{\mathrm{d}t} \tag{5}$$

Obviously Equation (5) can be expressed also in terms of the double layer charge only and then the problems with distinguishing between the integral and differential capacitance would not manifest themselves. However, in typical electrochemical practice it is more common, and also more convenient, to deal with the double layer capacitances data than with the double layer charges.

It is further noteworthy that the form of Equation (5) is strictly concordant with our concept of the $R_{\mathrm{s}}(R_{\mathrm{d}}C_{\mathrm{d}})$ equivalent circuit for the capacitive current at the streaming electrode in dc conditions [2], where R_{s} denotes the serial resistance of the circuit, whereas the branch corresponding to the permanent flow of the capacitive current is represented by the virtual resistor R_{d}. The circuit of an analogous con-

struction is given in Figure 1, but now, according to the Equation (5), the virtual R_d resistance is strictly related to the *integral* double layer capacitance K:

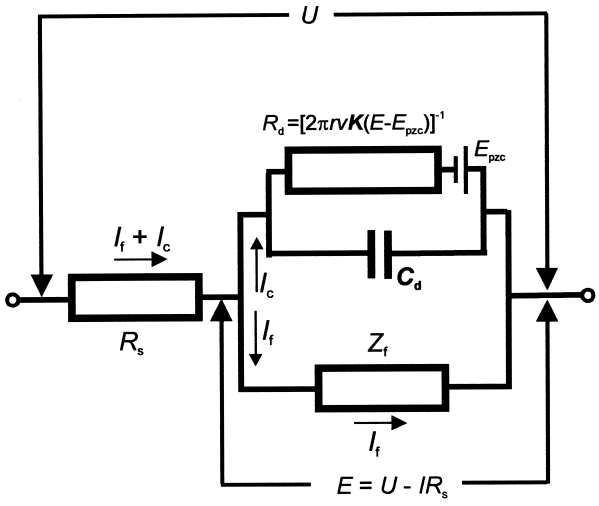

Figure 1. Equivalent circuit explaining the flow of the capacitive (I_c) and faradaic (I_f) currents at the streaming electrode in dc conditions. The total capacitive current splits into a branch with the virtual ohmic resistance R_d, dependent on the *integral* double layer capacitance K (through which the current flows at any potential E) and into the branch with the *differential* double layer capacitance C_d (through which the current flows only if $dE/dt \neq 0$). Other symbols: R_s – serial ohmic resistance, U – externally applied voltage, E – interfacial potential drop, smaller than U for the ohmic drops $(I_f + I_c)R_s$, E_{pzc} – potential of zero charge, r, v – radius and velocity of the mercury stream, respectively.

$$R_d = \frac{1}{2\pi rKv} \tag{6}$$

In conjunction with the definition of R_d one should also note that if this quantity is being determined from the ac measurements (impedance spectroscopy), it is related to the *differential* capacitance C_d [6] instead of the integral one. Nevertheless, since here we discuss only dc conditions, the definition of R_d given by Equation (6) will remain valid throughout the whole present paper.

In view of Equation (5) it becomes clear that if, for the simplification of theoretical analysis, we took into account only constant C_d [2] or only constant K [3] capacitance, we made an approximation – with respect to the contribution from either the permanent $2\pi rvK(E)\times(E\text{-}E_{pzc})$ or the instantaneous $2\pi rl_{max}C_d(E)\times(dE/dt)$ capacitive current, the latter one associated only with the small perturbation of the electrode potential. Now, based on Equation (5) and Equation (6) one can re-derive the stability criteria in the more strict forms than those given in Ref. [2] and make new calculations for the model electrode process:

$$\mathrm{Ox} + n\mathrm{e} \underset{k_\mathrm{b}}{\overset{k_\mathrm{f}}{\rightleftharpoons}} \mathrm{Red} \tag{7}$$

with the rate constants dependent on the electrode potential in this way that the I_f-E characteristics of the Ox electroreduction (with no Red species initially present) exhibit the region of the negative polarization resistance, followed by the increase of current at more negative potentials [1–3,5,6]. In this paper there will be used the dependence of k_f and k_b on the electrode potential E determined for the electroreduction of Ni(II)-SCN^- electroreduction at the streaming mercury electrode [1].

Stability criterion in the one-dimensional (1-D) case. In the one-dimensional case the electrode potential is the only dynamical variable considered and the change of the stability of the possible steady-states is associated with the monostable ⇔ multistable transitions, corresponding to the (degenerate) saddle-node bifurcations. The derivations analogous to those described in [2] lead to the following condition for the time dynamics of the electrode potential:

$$\frac{\mathrm{d}E}{\mathrm{d}t} = \frac{U-E}{2\pi r R_\mathrm{s} l_\mathrm{max}}\left(\frac{1}{C_\mathrm{d}}\right) - \frac{(E-E_\mathrm{pzc})v}{l_\mathrm{max}}\left(\frac{\boldsymbol{K}}{\boldsymbol{C}_\mathbf{d}}\right) - \frac{I_\mathrm{f}(E)}{2\pi r l_\mathrm{max}}\left(\frac{1}{C_\mathrm{d}}\right) \tag{8}$$

where $I_\mathrm{f}(E)$ is the faradaic current flowing at the electrode potential E, U is the externally applied voltage, and R_s is the serial ohmic resistance that causes the ohmic potential drop $(I_\mathrm{f}+I_\mathrm{c})R_\mathrm{s} = U\text{-}E$ (cf. Figure 1). It should be noted that the right-hand-side of Equation (8) differs from that of Equation (9) in Ref. [2] for the presence, in the middle term, of the factor (K/C_d), previously not given explicitly but implicitly always equal to unity, due to above-mentioned simplified assumption on the equality of differential and integral double layer capacitances. According to the principles of the linear stability analysis [10,11], the linearized system's response toward the small perturbation $\delta E = E - E_\mathrm{ss}$ of the steady-state electrode potential E_ss leads further to the following dependence for the time evolution of perturbations:

$$\frac{\mathrm{d}(\delta E)}{\mathrm{d}t} = -\frac{\delta E}{2\pi r l_\mathrm{max} C_\mathrm{d}}\left[\frac{1}{R_\mathrm{s}} + \frac{1}{Z_\mathrm{f}} + 2\pi r K v\right] \tag{9}$$

with Z_f (sometimes called the "zero-frequency faradaic impedance") denoting the slope $(\mathrm{d}E/\mathrm{d}I_\mathrm{f})_\mathrm{ss}$ of the I_f-E curve around the given steady-state. The instability of the steady-state potential requires the positive sign of the $\mathrm{d}(\delta E)/\mathrm{d}t$ derivative, what implies the negative sign of the expression in the square bracket:

$$\frac{1}{R_\mathrm{s}} + \frac{1}{Z_\mathrm{f}} + 2\pi r K v \equiv \frac{1}{R_\mathrm{s}} + \frac{1}{Z_\mathrm{f}} + \frac{1}{R_\mathrm{d}} < 0 \tag{10}$$

Thus, this instability condition differs from criterion derived in Ref. [2] only with the definition of R_d, now related strictly to the *integral* double layer capacitance, according to Equation (6).

Stability criterion in the two-dimensional (2-D) case. When both the electrode potential E and the surface concentration of the electroactive species $c_s \equiv c_{ox}(0,t)$ are considered the coupled dynamical variables, not only multistability but also oscillations can be diagnosed. Based on the same assumptions as in [2], but including now the difference between the differential and the integral double layer capacitance one obtains the system of the following autonomous differential equations:

$$\frac{\mathrm{d}E}{\mathrm{d}t} = \frac{U-E}{2\pi r R_s l_{max}}\left(\frac{1}{C_d}\right) - \frac{(E-E_{pzc})v}{l_{max}}\left(\frac{\boldsymbol{K}}{\boldsymbol{C_d}}\right) + nFk_f c_{ox}(0,t)\left(\frac{1}{C_d}\right) \equiv \mathrm{F}[E(t), c_{ox}(0,t)] \quad (11)$$

$$\frac{\mathrm{d}c_{ox}(0,t)}{\mathrm{d}t} = -\frac{2k_f c_{ox}(0,t)}{\overline{\delta_N}} + \frac{2D_{ox}[c_{ox}^0 - c_{ox}(0,t)]}{\overline{\delta_N}^2} \equiv \mathrm{G}[E(t), c_{ox}(0,t)] \quad (12)$$

The combination of Equations (11) and (12), with the simultaneously imposed conditions $\mathrm{d}E/\mathrm{d}t = \mathrm{d}c_s/\mathrm{d}t = 0$, leads to expression (13):

$$\frac{U-E_{ss}}{2\pi r R_s C_d l_{max}} - \frac{(E_{ss}-E_{pzc})v}{l_{max}}\left(\frac{\boldsymbol{K}}{\boldsymbol{C_d}}\right) + \frac{nFk_f(E_{ss})c_{ox}^0 D_{ox}}{C_d[D_{ox} + k_f(E_{ss})\overline{\delta_N}]} = 0 \quad (13)$$

from which the steady-state potential E_{ss} (and hence also the corresponding steady-state concentration c_{ss}) can be calculated, *i.e.* the possible steady-states of the dynamical system (11,12) for given (U, R_s) control parameters can be found.

According to the principles of the linear stability analysis [10] the possible bifurcations of these steady-states can be diagnosed from the characteristics of the Jacobian matrix **J** (14), in which the new (K/C_d) term appears as the factor in the middle term of the a_{11} element.

$$\mathbf{J} = \begin{bmatrix} a_{11} & a_{12} \\ a_{21} & a_{22} \end{bmatrix} = \begin{bmatrix} \left(\frac{\partial \mathrm{F}}{\partial E}\right)_{ss} & \left(\frac{\partial \mathrm{F}}{\partial c_s}\right)_{ss} \\ \left(\frac{\partial \mathrm{G}}{\partial E}\right)_{ss} & \left(\frac{\partial \mathrm{G}}{\partial c_s}\right)_{ss} \end{bmatrix}$$

$$= \begin{bmatrix} \frac{-1}{2\pi r R_s C_d l_{max}} - \frac{v}{l_{max}}\left(\frac{\boldsymbol{K}}{\boldsymbol{C_d}}\right) + \frac{nFc_{ss}}{C_d}\left(\frac{\mathrm{d}k_f}{\mathrm{d}E}\right)_{ss} & \frac{nFk_f(E_{ss})}{C_d} \\ -\frac{2c_{ss}}{\overline{\delta_N}}\left(\frac{\mathrm{d}k_f}{\mathrm{d}E}\right)_{ss} & -\frac{2k_f(E_{ss})}{\overline{\delta_N}} - \frac{2D_{ox}}{\overline{\delta_N}^2} \end{bmatrix} \quad (14)$$

The saddle-node bifurcation occurs when the determinant $Det(\mathbf{J}) = 0$, whereas the Hopf bifurcation corresponds to the condition: trace $Tr(\mathbf{J}) = 0$, with $Det(\mathbf{J}) > 0$. Based on the characteristics of matrix (14) it is now possible to check quantitatively, how much the shape of the bifurcation diagram of the Ni(II)-SCN^- electroreduction is determined by: (i) contribution of the permanently flowing capacitive current, including the role of the (K/C_d) factor and (ii) the thickness of the diffusion layer.

RESULTS AND DISCUSSION

The role of (K/C_d) term in the shape of the bifurcation diagram. The present analysis will be limited to a two-dimensional case, as being more realistic for our experimental example: Ni(II)-SCN^- electroreduction, exhibiting both oscillations and bistability. Both $C_d(E)$ and the corresponding calculated $K(E)$ dependencies for 2 mol dm^{-3} NaSCN are plotted in Figure 2-A, whereas Figure 2-B shows the K/C_d *vs.* E dependence.

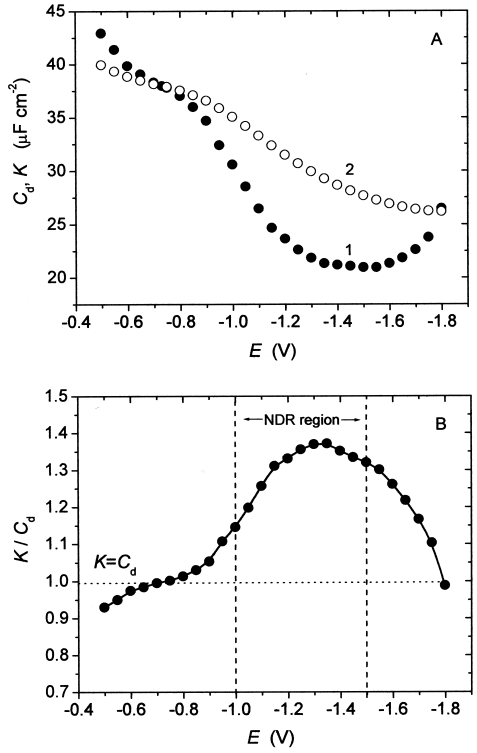

Figure 2. (A) Differential C_d (1) and integral K (2) double layer capacitances of the mercury electrode in contact with 2.0 mol dm^{-3} NaSCN, as a function of the electrode potential (*vs.* the saturated (KCl) calomel electrode); (B) the corresponding (K/C_d) *vs.* E dependence, with the indicated approximate potential interval corresponding to the region of the negative differential resistance (NDR) in the *I-E* characteristics [1] of the electroreduction of 5.0 mmol dm^{-3} $Ni(ClO_4)_2$ + 2.0 mol dm^{-3} NaSCN at a streaming mercury electrode.

A very strict analysis of the role of the (K/C_d) factor in the system's stability should obviously involve the exact dependence of the differential and integral double layer capacitances on the electrode potential, what would significantly complicate numerical calculations. However, as we show below, for drawing the principal conclusions it is sufficient to invoke different *constant* values of C_d and K quantities. For that purpose from Figure 2 we chose the values of C_d and K exhibiting the *maximum* difference, i.e.: $C_d = 21.86\,\mu$F cm^{-2} and $K = 29.95\,\mu$F cm^{-2} corresponding to the electrode potential $E = -1.3$ V (note that this potential is located within the region of NDR which is penetrated by the system in the oscillatory or multistable regime). The maximum K/C_d value is thus equal to 1.37, and it is logical to expect that the effect of the K/C_d ratio less than this limiting value can only be smaller. This approach will reveal how sensitive toward realistic differences between K and C_d the discussed stability criteria are.

The bifurcation diagrams constructed by us for various combinations of K and C_d are shown in Figure 3 where (for better legibility) they are separated into sets of points corresponding to the Hopf and the saddle-node bifurcations. If all the diagrams were

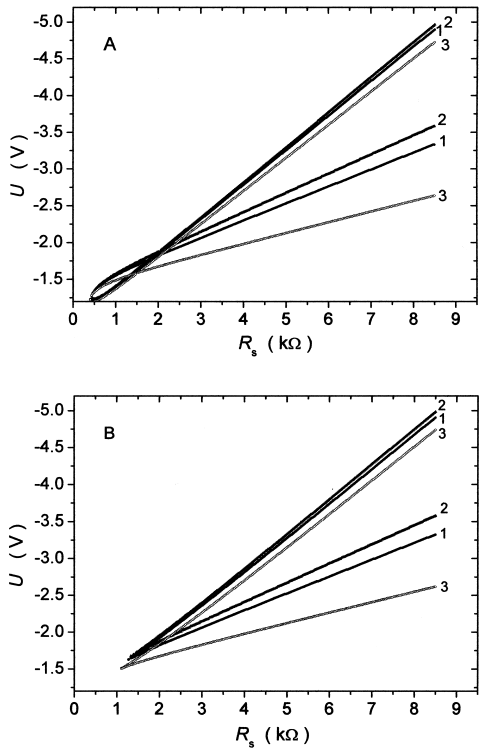

Figure 3. Separated into two Figures points of the (A) Hopf and (B) saddle-node bifurcations for the dynamical system (11, 12), calculated for various combinations of the differential and integral double layer capacitance: (1) $C_d = K = 21.86\,\mu$F cm^{-2}, (2) $C_d = 21.86\,\mu$F cm^{-2}, $K = 29.95\,\mu$F cm^{-2}, (3) $K = 0$, $C_d = 21.86\,\mu$F cm^{-2}.

presented in the same coordination system, as in principle it should be done for the unambiguous description of the dynamical properties of the process considered, they all would resemble the diagram in Figure 6-A in Ref. [2]. These diagrams show that as long as the K and C_d capacitances keep realistic values (what is the case for curves (1) and (2)), the plots for different (K/C_d) ratios are quite close to each other. This means also that all our previous simplified assumptions [1–3] were reasonable and justified. However, in this paper we analyse the role of the K/C_d ratio in the d.c. measurements only, whereas its significance for the diagnosis of the system's stability from the impedance spectra will be the discussed in another study [12].

The role of the permanent capacitive current (v/l_{max} term) in the shape of the bifurcation diagram. Curves (3) in Figure 3 show that if $K = 0$, *i.e.* when the contribution of the flow term v/l_{max} to the a_{11} element of the Jacobian matrix is totally eliminated, the points of the saddle-node bifurcation distinctly change their position in the (U,R_s) phase space, with the oscillatory region getting simultaneously a bit smaller.

The physical sense of the effect of the v/l_{max} term on the *bistable* region can be easily understood from the analysis of the *I-E* characteristics of the Ni(II)-SCN^- electroreduction, with the permanent capacitive current I_c taken into account or – for comparison – neglected. Figure 4 illustrates the principle of this explanation for the exemplary constant serial resistance R_s = 5.5 kΩ and varying external voltage U. The multiple steady states exist within the parameter U region characterised with multiple points of intersection of this *I-E* characteristics with the load lines $I = U/R_s$ –

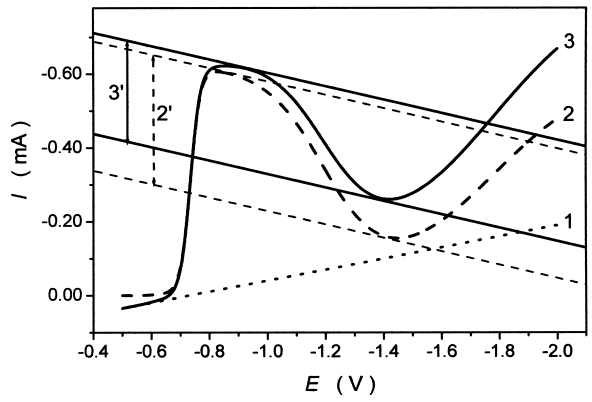

Figure 4. Explanation of the effect of permanently flowing capacitive current on the region of the control parameter U corresponding to the bistable behaviour in the Ni(II)-SCN^- electroreduction at the streaming electrode. Curves: (1) calculated capacitive current; (2) calculated faradaic current; (3) total (1+2) current. The *I-E* characteristics for the faradaic and the total currents intersect with the respective load lines $I = U/R_s - E/R_s$ (for R_s = 5.5 kΩ and varying U) showing that in the absence of the permanent capacitive current the bistability would occur within region (2'), for $U \in$ (–2.26 V, –4.19 V), whereas in the presence of this current it is (as in reality) observed within the region (3'), for $U \in$ (–2.81 V, –4.32 V) (cf. Figure 3 for comparison). For numerical parameters of calculations, see Ref. [2].

E/R_s. In Figure 4 the steady-state faradaic current I_f of the electrode process considered was calculated from the analytical expression [2]:

$$I_f = -2\pi rnFc_{ox}^0 k_f v\left[\frac{2}{\kappa}\sqrt{\frac{t_{max}}{\pi}} + \frac{\exp(\kappa^2 t_{max})\mathrm{erfc}(\kappa t_{max}^{1/2}) - 1}{\kappa^2}\right] \quad (15)$$

where the maximum electrolysis time at the streaming electrode $t_{max} = l_{max}/v$.

In turn, the fact that the *oscillatory* region does not significantly change its position and size, suggests only a relatively minor effect of the background capacitive current on the coupled dynamics of the electrode potential E and of the surface concentration c_s, at least for our experimental conditions. In fact, the numerical integration of Equations (11,12), for the exemplary (U, R_s) parameters corresponding to the oscillatory regions from curves 1 and 3 in Figure 3-A shows that the absence of the $(K/C_d)(v/l_{max})$ term causes a slight only increase in both the amplitude and the period of oscillations (see Figure 5). The period of both these oscillatory courses is anyway significantly shorter than that observed in the experiment [1], which fact is a

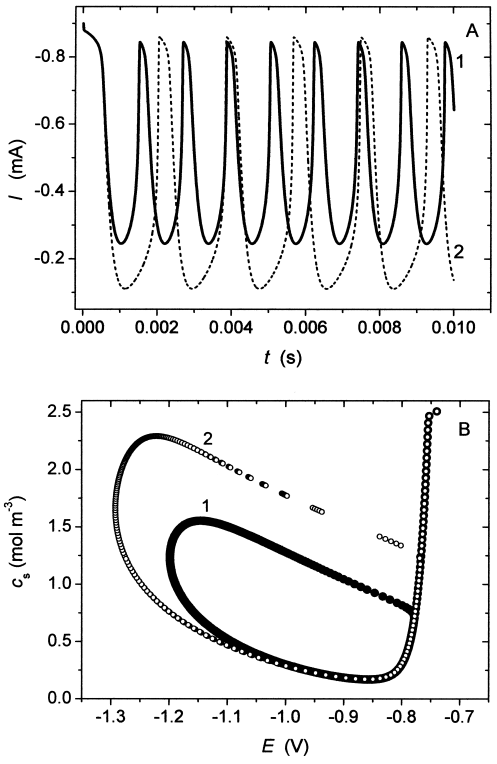

Figure 5. (A) Model oscillations of the total current I of the Ni(II)-SCN^- electroreduction obtained from numerical integration of Equations (11, 12) by the fourth-order Runge-Kutta method with the automatic step-size correction [13]), for (1): $K/C_d = 1.37$ and (2) $K = 0$; (B) the corresponding (1, 2) limit cycles. Parameters: $U = -1.370$ V, $R_s = 700\ \Omega$.

consequence of simplifications underlying the derivation of Equations (11, 12) (mainly the approximation of the real diffusion profile by the linear one).

In order to explain the role of v/l_{max} term more quantitatively, in Table 1 we collected exemplary values of all the three terms (T_1, T_2, T_3) composing the a_{11} element of the Jacobian matrix (14), as well as – for intercomparison – of all its a_{ij} elements. It appears that the discussed $T_2 = -v/l_{max}$ term is comparable to or *lower* than term T_1, and they both are significantly lower than the T_3 term. From these numerical values it follows that the significant effect of the (v/l_{max}) term (and thus of the K/C_d ratio, either) on the bifurcation diagram could be theoretically expected, if the mercury flow velocity v were appropriately higher than applied by us. However, enhancing v causes the simultaneous decrease in the (average) thickness of the diffusion layer. The role of the thickness of the diffusion layer will be analysed below in more detail.

Table 1. Exemplary values of the terms T_1, T_2, T_3 composing the $a_{11} \equiv T_1 + T_2 + T_3$ element and all a_{ij} elements of the Jacobian matrix (14) for selected steady-states, close to the positions of the saddle-node bifurcation points (1) from Figure 3-B.

U / V	R_s / Ω	$10^{-3}\times T_1$ / s^{-1} (a)	$10^{-3}\times T_2$ / s^{-1} (b) = const.	$10^{-3}\times T_3$ / s^{-1} (c)	$10^{-3}\times a_{11}$ / s^{-1}	$10^{-3}\times a_{12}$ / s^{-1}	$10^{-3}\times a_{21}$ / s^{-1}	$10^{-3}\times a_{22}$ / s^{-1}
–1.740	1570	–3.373	–0.650	15.72	11.70	1.31	–29.68	–3.41
–2.600	3530	–1.500	–0.650	19.81	17.66	3.84	–37.40	–8.19
–3.013	4440	–1.193	–0.650	19.96	18.12	4.09	–37.69	–8.66
–4.020	6610	–0.801	–0.650	20.68	19.23	5.81	–39.04	–11.91
–4.900	8500	–0.623	–0.650	20.82	19.55	6.34	–39.32	–12.92

[a] $$T_1 = \frac{-1}{2\pi r R_s C_d l_{max}}$$

[b] $$T_2 = -\frac{v}{l_{max}}\left(\frac{K}{C_d}\right)$$

[c] $$T_3 = \frac{nFc_{ss}}{C_d}\left(\frac{dk_f}{dE}\right)_{ss}$$

One should note that the analysis of the case $K = 0$ shows which the system's behaviour would be, if it were possible to study the same process at the electrode which does not undergo a permanent charging, as e.g. at the solid, rotating disc electrode (covered with mercury layer in this case), with a rotation speed adjusted so that the thickness of the diffusion layer in solution is the same as the average thickness of that layer at the streaming electrode. Thus, the case $K = 0$ does not correspond to a completely abstract, unrealistic situation.

The role of the thickness of the diffusion layer ($\overline{\delta_N}$) in the shape of the bifurcation diagram. Further analysis of the properties of matrix **J** leads to the conclusion that the shape of the stability diagrams from Figure 3 is determined also by a very small, compared to the typical non-streaming electrodes, thickness of the diffusion layer $\overline{\delta_N}$, included in the elements a_{21} and a_{22} of the Jacobian matrix (14). The a_{21} element affects the value of the determinant, and the a_{22} element affects both the trace and the determinant of matrix **J**, in this way contributing to the positions of the points of both bifurcations considered. The simplest way of modifying the thickness of the diffusion layer in the experiment is to change the flow velocity of mercury (v), but then obviously v/l_{max} term also changes its value. For the exemplary illustration of the interplay of these two effects, in Figure 6-A we compare the realistic bifurcation diagram (1) for the Ni(II)-SCN^- electroreduction, composed of

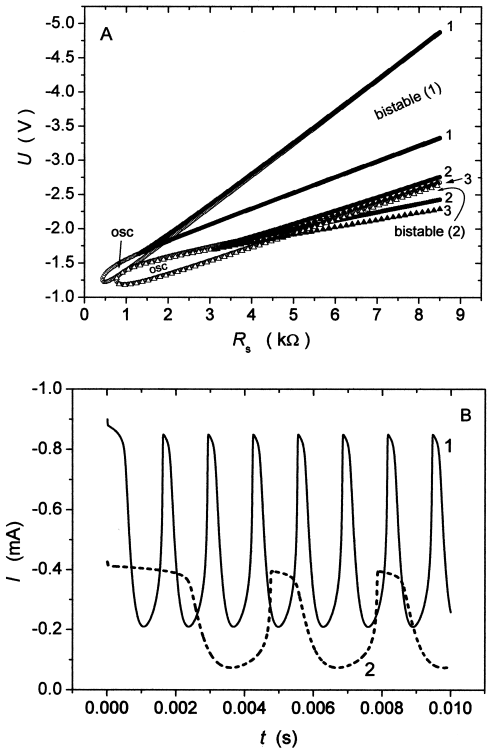

Figure 6. (A) Comparison of the full theoretical bifurcation diagrams of the Ni(II)-SCN^- electroreduction for the mercury stream velocity: (1) v = 1.620 m s^{-1} (experimental case) and (2) v = 0.324 m s^{-1} (theoretical case), with all other parameters identical and corresponding to points (1) in Figure 3. For confirmation of a negligible role of the v/l_{max} term in case (2), points (3, ▲, △) show the course of the diagram (2) with the imposed additional condition K = 0; (B) comparison of the model oscillatory I = f(t) courses, corresponding to diagrams (1) and (2) from part (A), obtained from the numerical integration of Equations (11, 12) for: (1) U = –1.370 V, R_s = 700 Ω and (2) U = –1.367 V, R_s = 1520 Ω.

points (1) from Figures 3-A and 3-B, with the diagram (2) calculated for the velocity of mercury stream v lower for the factor 0.2 than for curve (1) (note that in practice it may be difficult to prepare the streaming electrode working satisfactorily with such a low flow rate, and thus the rate of the reactant transport may be varied only within a rather limited range). For diagram (2) the v/l_{max} term decreases then from 650 to 130, whereas the mean thickness of the Nernst diffusion layer $\delta_N = (2/3)(\pi D_{ox} t_{max})^{1/2}$ [2] rises from 1.21 μm to 2.70 μm. The difference in bifurcation diagrams is now pronounced more strongly than in Figure 3. For the decreased transport rate of the reactant towards the electrode surface the oscillatory region becomes significantly larger, showing that the relation between the time scales of the dynamics of the electrode potential E and of the dynamics of surface concentration c_s of the reactant significantly changed. Figure 6-B shows the simultaneous, also rather significant change in the amplitude and the period of oscillations.

In turn, the bistable region becomes now significantly narrower and undergoes a substantial shift in the phase space. According to explanation illustrated earlier in terms of Figure 4, it is a result of the modification of the N-shaped I-E characteristics of the circuit: now, for the lower transport rate the background, capacitive current is appropriately lower, but also the minimum formed by the kinetically controlled faradaic current is less pronounced. In order to prove which is the effect of the simultaneous change of the v/l_{max} term, in Figure 6-A we show the additional curve (3) corresponding, as curve (2), to $\delta_N = 2.70$ μm, but with the imposed condition $K = 0$. Curves (3) are located in the phase space very closely to curves (2), so it becomes clear that the change of diagram (1) to diagram (2) was caused largely by the decrease in δ_N.

CONCLUSIONS

Concluding, in the above analysis we derived the more strict stability criteria than before [2] and showed the role of two factors, specific to the streaming electrodes: the permanent flow of the capacitive current and the relatively small thickness of the diffusion layer, in determination of the conditions for oscillations and bistability, for the Ni(II)-SCN^- electroreduction as an example. For the given experimental characteristics of both the streaming electrode and the redox system studied, both factors were found to determine the shape of the bifurcation diagram and the characteristics of oscillations, with the predominant role of a relatively thin diffusion layer. One may expect that with increasing flow rate of mercury and decreasing bulk concentration of the reactant the role of the permanent capacitive current in the dynamical properties of the system will become more significant.

Since electrochemical properties of the Ni(II)-SCN^- system, possessing the NDR region in its I-E characteristics, are quite typical of electrode reactions exhibiting dynamical instabilities, the conclusions drawn in this paper should be applicable also for other processes of that type, if studied at the streaming electrodes. In our opinion,

since the streaming mercury electrode is a very powerful tool for studying oscillations and multistability in electrode processes, its specific properties are worth of detailed analysis, and a part of such an analysis was presented in this paper.

REFERENCES

1. Jurczakowski R. and Orlik M., *J. Phys. Chem. B*, **10**6, 1058 (2002).
2. Orlik M. and Jurczakowski R., *J. Phys. Chem. B*, **106**, 7527 (2002).
3. Jurczakowski R. and Orlik M., *J. Phys. Chem. B*, **107**, 10148 (2003).
4. Heyrovský J. and Forejt J., *Z. Physik. Chem*., **193**, 77 (1947).
5. Jurczakowski R. and Orlik M., *J. Electroanal. Chem.*, **486**, 65 (2000).
6. Jurczakowski R. and Orlik M., *J. Electroanal. Chem*., **562**, 205 (2004).
7. Electroanalytical Methods of Determination of Physicochemical Constants, Ed. Z Galus, PWN, Warsaw, 1979 (*in Polish*).
8. Bard A.J. and Faulkner L.R., Electrochemical Methods. Fundamentals and Applications, second ed., Wiley, New York, 2001, p. 541.
9. Delahay P., *J. Electroanal. Chem*., **10**, 1 (1965).
10. Strogatz S.H., Nonlinear Dynamics and Chaos, Addison-Wesley: Reading, MA, 1994.
11. Koper M.T.M., *Electrochim. Acta*, **37**, 1771 (1992).
12. Jurczakowski R. and Orlik M., in preparation.
13. Marciniak A., Gregulec D. and Kaczmarek J., Numerical Procedures in Turbo Pascal for Your PC, Nakom, Poznań, 1991.